Journal of Applied Polymer Science

Polymeric piezoelectric fiber with metal core produced by electrowetting-aided dry spinning method

Weiting Liu, Ran Chen, Xiaodong Ruan, Xin Fu
The State Key Laboratory of Fluid Power & Mechatronic Systems, Zhejiang University, Zheda Rd. 38, Hangzhou, China
Correspondence to: R. Chen (E-mail: yuukyuu@zju.edu.cn)

ABSTRACT: An electrowetting-aided dry spinning method is developed to produce morphologically stable polymeric piezoelectric fibers with a metal core covered by a beta-phase poly(vinylidene fluoride) [or poly(vinylidene-trifluoroethylene)] layer. Each fiber consists of a 100 μm copper core (enameled with 6 μm polyester-imide), a 3–10 μm piezoelectric layer, and a sputtered 100 nm gold electrode. The morphological properties of the fibers are analyzed with scanning electron microscopy, X-ray diffraction, and a step profiler. The piezoelectric properties are tested in a vibration-detecting application. Both morphological observation and piezoelectric testing demonstrate that the electrowetting-aided dry spinning helps in forming high-quality polymeric piezoelectric fibers. Moreover, this method can also be applied in different fabrications, where adhesion between a liquid and solid surface needs to be enhanced.
 J. Appl. Polym. Sci. **2016**, *133*, 43968.

KEYWORDS: dielectric properties; fibers; morphology; sensors and actuators

Received 12 January 2016; accepted 24 May 2016
DOI: 10.1002/app.43968

INTRODUCTION

Piezoelectric fibers with a metal core are considered as a solution to overcome the shortcomings of full polymeric sensing ones with a couple of electrodes on the surface: the array substrate can be conductive or not, fibers can be applied on more complex shapes, and all fibers can be used independently to keep the system working properly even if some fibers fail.

In recent years, efforts have been made in the research on metal-core piezoelectric fibers, mostly related to ceramic fibers. For example, Qiu *et al.*[1] and Sato *et al.*[2] have produced lead zirconate titanate (PZT) fiber with a metal core serving as an inner electrode by extruding a mixture of PZT powder and organic solvent together with the metal core. Since then, further research has been carried out to investigate the detailed properties of these piezoelectric fibers. Sebald *et al.*[3] analyzed the first resonance mode and found the existence of an optimal diameter at which the pseudolateral coupling factor is maximal. Sato *et al.*[4] designed a smart board by mounting these piezoelectric fibers onto the surface of a carbon fiber–reinforced plastic composite, and Takagi *et al.*[5,6] developed the vibration-control and damage-detection method for this smart board. Yanaseko *et al.*[7,8] developed a metal-core piezoelectric ceramic fiber–aluminum composite, which can be applied as a wireless strain sensor owing to its strain-measurement and energy-harvesting capabilities.

Poly(vinylidene fluoride) (PVDF) and poly(vinylidene-trifluoroethylene) (PVDF-TrFE), with excellent ferroelectricity and high strain level,[9–11] have attracted lots of attention. Compared to the ceramic piezoelectric materials, one advantage of PVDF and PVDF-TrFE is their flexibility,[12] which makes them suitable for wearable applications.[13]

To date, the fabrication of PVDF and PVDF-TrFE fibers with conductive cores can for the most part be classified into two methods: coaxial melt spinning and tensile melt extruding. Coaxial melt spinning is a popular method to produce fibers with a core–sheath structure. By adding conductive particles into the core polymer and using PVDF (or PVDF-TrFE) as a sheath material, PVDF (or PVDF-TrFE) fiber with a conductive core can be generated. For example, Lund *et al.*[14,15] developed PVDF fiber with a conductive carbon black–polypropylene core and studied the effects of parameters. Glauß *et al.*[16] produced PVDF fiber with a carbon nanotube–doped polypropylene core. Tensile melt extruding is another effective way to generate metal-core PVDF and PVDF-TrFE fibers.[17,18] This method first places a metal filament in the center of melting PVDF or PVDF-TrFE, and then extrudes the polymer along with pulling the metal filament. Because the metal filament is kept in the center, PVDF or PVDF-TrFE fiber with metal core can be finally produced.

However, both methods still have their drawbacks. For coaxial melt spinning, a conductive core fabricated by adding conductive particles into the polymer usually has very high resistance; for tensile melt extruding, it is difficult to ensure a perfect

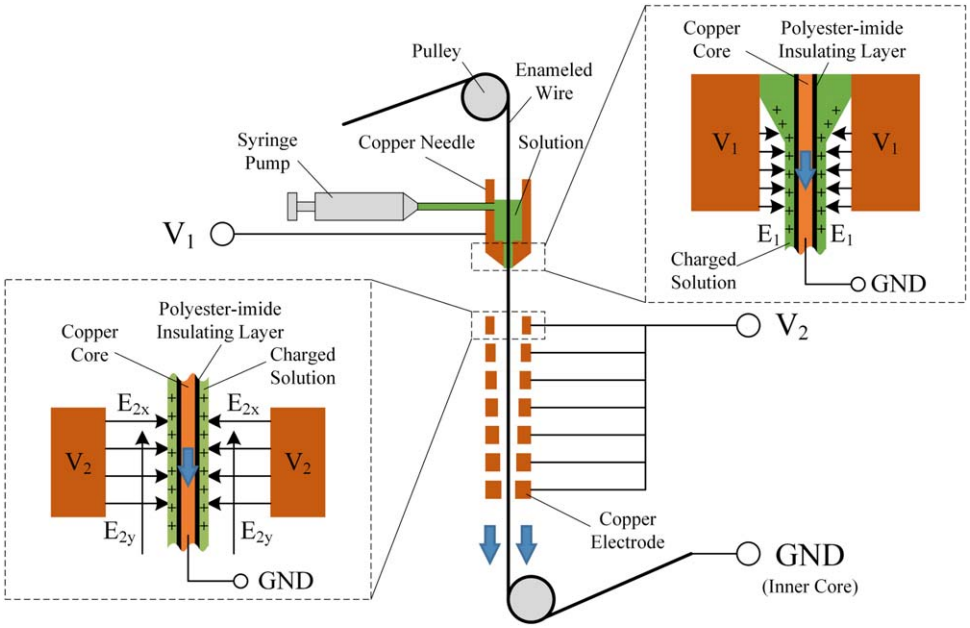

Figure 1. Schematic of the piezoelectric fiber fabricating device. [Color figure can be viewed in the online issue, which is available at wileyonlinelibrary.com.]

integration of the piezoelectric layer and metal core, due to less strong adhesion between melt polymer and metal surface, without pretreatment and preheating.[19] Meanwhile, these methods usually generate a thick piezoelectric layer (more than 20 μm); although a thicker piezoelectric layer leads to greater response,[20] it also usually induces a more nonlinear response because of the viscoelasticity of the polymer layer.

By using PVDF and PVDF-TrFE solutions instead of a melt, the thickness of the piezoelectric layer can be definitely decreased, whereas there is still left the problem of polymer-to-metal adhesion. Electrowetting, referring to techniques in which the apparent wettability of liquids can be controlled by applying an external electric potential,[21–25] is considered available to strengthen the interfacial adhesion between the polymeric piezoelectric material and the solid surface. Besides, in the experiment of PVDF electrospinning, fabrication with an electric field driving elongation has been proven as an effective method to form the beta phase.[26] Thus, the application of an electric field during the solidification is proposed.

In this paper, a polyester-imide enameled wire is selected to be the core of the piezoelectric fiber. The enamel can serve as an essential insulating layer in electrowetting as well as improve the adhesion of PVDF or PVDF-TrFE. An external electric potential is applied to the core to improve its wettability when the moving wire carries out the PVDF (or PVDF-TrFE) solution so as to produce a morphologically stable piezoelectric fiber. Meanwhile, other electric fields are applied during the solidification of the solution to keep the fiber shape and promote further beta phase transition and polarization of the PVDF layer, which can be validated in the fiber characterization. Finally, fabricated fibers with a thin piezoelectric layer (from 3 μm to 10 μm in different concentrations) are packaged and tested. Vibration testing of the fiber shows high sensitivity (more than 200 pC at 500 Hz in 1 mm vibrating amplitude) if considering the piezoelectric layer's thickness.

EXPERIMENTAL

Materials

We use PVDF and PVDF-TrFE as the piezoelectric fiber sheath. PVDF powder (average $M_w = 534{,}000$) was purchased from Sigma-Aldrich (St. Louis, Missouri, United States). PVDF-TrFE (70–30 mol %) was purchased from Piezotech (Pierre-Benite Cedex, France). Acetone and dimethyl formamide (DMF) were purchased from Sinopharm Chemical Reagent (Shanghai, China). Poly(tetrafluoroethylene) (PTFE) heat shrink tube (Sub-Lite-Wall) was purchased from Zeus (Orangeburg, South Carolina, United States). Polyester-imide enameled wire (with 100 μm diameter copper core and 6 μm thick polyester-imide insulating layer) was purchased from Zhengzhou LP Industry (Zhengzhou, Henan, China). Enamel remover (HJ-202T) was purchased from Huajin Electro (Dongguan, Guangdong, China) to expose the copper core.

Piezoelectric Fiber Fabrication

A schematic of the piezoelectric fiber fabricating device is shown in Figure 1. A polyester-imide enameled wire with 100 μm diameter copper core and 6 μm thick polyester-imide insulating layer is used as the substrate. The polyester-imide insulating layer serves as an essential part in electrowetting and enhances the adhesion of PVDF (or PVDF-TrFE). This enameled wire is located by a couple of pulleys and passes through the center of a copper needle (1 mm tip aperture) and a series of copper electrodes with inner diameter varying from 3.5 mm to 0.5 mm. The solution is continuously supplied into the copper needle by a syringe pump (Braintree Scientific BS-9000-6, Braintree, Massachusetts, United States) and then exposed to the atmosphere.

As shown in Figure 2(a), the fiber is fabricated by the electrowetting-aided dry spinning method. When the fabrication is starting, the enameled wire is pulled by a motor and the copper core is grounded. A high-voltage power supply (V_1) generates an electric field (E_1)

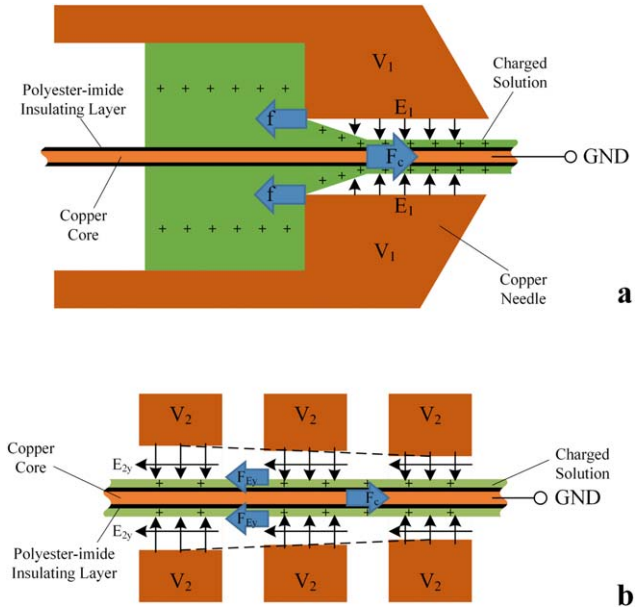

Figure 2. Schematic of the detailed fabricating process. [Color figure can be viewed in the online issue, which is available at wileyonlinelibrary.com.]

from the cylindrical copper needle to the enameled wire and positively charges the solution. The electric charge will be stored in the solution throughout the whole fabrication process, owing to the insulation of the polyester-imide layer. Because of the force that results from the applied electric field, the wettability increases and the solution adheres to the surface of the enameled wire more strongly. As the enameled wire keeps moving, the resistance force (f) from the orifice and the enhanced adhesion force (F_c) work together to perform a stretching process, during which the charged solution undergoes solidification, and therefore the resultant piezoelectric layer is elongated. Finally the solution under solidification is carried out of the copper needle together with the enameled wire.

As shown in Figure 2(b), after moving out of the copper needle, the enameled wire passes through a series of copper electrodes with reducing inner diameter. These electrodes are connected to another high-voltage power supply (V_2) and apply other electric fields on the solution. As the inner diameter of the copper electrode decreases along the enameled wire, in addition to the electric fields vertical to the wire axis that polarize the piezoelectric layer and improve the morphological stability, electric fields parallel to the wire axis (E_{2y}) are also generated. Thus the electric force from the parallel electric fields (F_{Ey}) can work together with the adhesion force (F_c) to make a positively charged solution perform further deformation under solidification.

For PVDF, in addition to the phase transition that is due to the very high electric field,[13,15] the elongation and further deforming process are also considered to form the beta phase, which is linked to the PVDF electrospinning process[26] and the well-known fact that an obvious increase of the beta phase is observed after the stretching of alpha-phase PVDF films at temperatures below 90 °C.[27] For PVDF-TrFE, it has been proven that with 20–50 mol % TrFE this copolymer tends to generate the beta phase below the melting point.[28] Therefore, through this electrowetting-aided dry spinning method, morphologically stable fibers with a well-distributed beta-phase piezoelectric layer can be achieved.

In our fabrication, 10 wt %, 15 wt %, and 20 wt % solutions are prepared by dissolution of PVDF or PVDF-TrFE in a 1:1 DMF/acetone mixture. The moving speed of the enameled wire is adjusted to be 200 mm s^{-1}, and the solution flow rate is set as 0.1 mL min^{-1}. The voltage V_1 is set to be 1 KV and the voltage V_2 is 4 KV. Finally, we successfully fabricate PVDF and PVDF-TrFE coated fibers at these three concentrations. For comparison, fibers with 15 wt % PVDF (marked as U15%PVDF) and 15 wt % PVDF-TrFE (marked as U15%PVDF-TrFE) layers have also been produced with no electric field applied during the fabrication.

Meanwhile, another experiment is carried out to find out the cause of the beta phase. As described before, during the fabrication of the piezoelectric fiber, the phase transition due to the electric field, as well as the elongation process, may contribute to the formation of the PVDF beta phase. However, for a solid PVDF film structure, the field strength required to achieve a phase transition is usually above 300 MV m^{-1},[29,30] which is much higher than the field strength applied in our experiments (less than 20 MV m^{-1}). Therefore, it is necessary to understand whether the lower electric field can contribute to the formation of the beta phase in the piezoelectric layer under solidification.

In this experiment, no voltage is applied to the copper needle ($V_1 = 0$), so the solution will not be charged, and the influence of elongation and further deforming processes can be almost excluded. The same device as in piezoelectric fiber fabrication is used, and the moving speed of the enameled wire (200 mm s^{-1}) and the solution flow rate (0.1 mL min^{-1}) are also the same as before. A 4 KV voltage (V_2) is still applied to the copper electrodes in the fabrication of another group of 15 wt % PVDF layer coated fibers (marked as NC15%PVDF) for comparison.

Characterization

Scanning electron microscopy (SEM) is performed to analyze the surface of the piezoelectric layer by using a Hitachi S4800 (Chiyoda, Tokyo, Japan) scanning electron microscope running at 3 kV.

The X-ray diffraction (XRD) patterns of the fibers are recorded by using a PANalytical (Almelo, The Netherlands) X'Pert PRO advanced diffractometer at room temperature. The X-ray source was Cu Kα radiation (wavelength 0.15406 nm, voltage 40 kV, and current 40 mA). The samples were scanned at a speed of 0.025° min^{-1} from 5° to 50°.

The diameters of the fibers are tested with a Bruker (Billerica, Massachusetts, United States) DEKTAK-XT step profiler. Five thicknesses of the piezoelectric layer at different positions are acquired by the difference of the diameters of the fabricated fiber and the original enameled wire.

Packaging Method

Fabricated piezoelectric fibers need electrode coating and packaging. First, after being fixed with a prepared clamp, the fibers are sent into a magnetron sputtering machine to coat a gold layer onto the whole length as outer electrodes. A gold layer

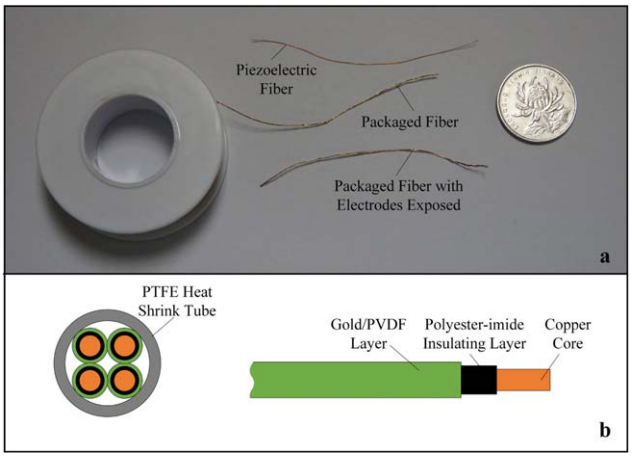

Figure 3. (a) Photo of piezoelectric fiber and packaged fiber. (b) Schematic of packaged fiber. [Color figure can be viewed in the online issue, which is available at wileyonlinelibrary.com.]

with a thickness of 100 nm is obtained through time- and power-controlled sputtering. Then, four fibers are twisted together and passed through a PTFE heat shrink tube. Finally, the tube is heated to shrink by a hot-air gun, and the fibers are packaged in the tube with a coverage thickness of 0.03 mm. Given the high efficiency of fabrication, the packaged fibers can be very long [a fiber with a length of 10 m twisted around a spool is shown in Figure 3(a)]. A photo and the structure of the packaged fiber are shown in Figure 3.

Before actual application, we need to cut a certain length and expose the electrodes. The heat-shrink tube should be cut off a little to expose the gold/PVDF layer. Then the fiber is dipped in DMF/acetone for a while to expose the insulating layer, and finally we remove the enamel with the enamel remover. The final state of each contained fiber is shown in Figure 3(b).

Test Setup

Packaged fibers are tested in a vibration-detecting application. The test setup is shown in Figure 4. A steel ruler is used as a cantilever with one side fixed and the other side connected to a shaking table (LDS V455, Brüel & Kjær, Nærum, Denmark). The tested fiber (with length of 60 mm) is adhered to this cantilever with double-sided tape, and the exposed electrodes of the tested fiber are connected to a charge amplifier (Donghua Test DH5862, Jingjiang, Jiangsu, China) through a pair of testing clamps. The output of the charge amplifier is acquired through a data-acquisition tool (DAQ, NI USB-6343), and after passing through a virtual band-stop filter (45–55 Hz), the signal is recorded in a computer. In order to achieve closed-loop feedback control, an acceleration sensor (PCB Piezotronics 352C33, Buffalo, New York, United States) is placed beside the center of the tested fiber. This sensor is connected to a controller (Crystal Instruments SPIDER-818, Santa Clara, California, United States), which sends the signal to the power amplifier (LDS PA1000L, Brüel & Kjær, Nærum, Denmark) and controls the vibration of the shaking table. Therefore, just by connecting the controller to a computer, control of the acceleration around the tested fiber can be easily achieved.

The vibration amplitude A at the test point can be obtained from the detected acceleration and frequency:

$$A = \frac{\varepsilon \max}{4\pi^2 f^2} \tag{1}$$

In this equation, A is the vibration amplitude, f is the frequency of vibration, and ε_{max} is the amplitude of acceleration.

Meanwhile, because the vibration spreads as a wave and the tested fiber deforms along with the wave, the strain amplitude of the tested fiberis

$$\varepsilon_{max} \approx \max\left(\frac{dA\,\sin\left(\frac{2\pi f}{v}x\right)}{dx}\right) = \frac{2\pi}{v} fA \tag{2}$$

where K is the wave velocity on the cantilever, which usually stays constant.

Therefore, if the detected charge quantity amplitudeis linearly proportional to the strain amplitude of the fiber, then

$$Q_{max} = k\varepsilon_{max} \approx KfA \tag{3}$$

$$\frac{Q_{max}}{A} \approx Kf \tag{4}$$

where K is a constant. Thus the charge quantity amplitude is linearly proportional to the product of the vibration amplitude and frequency.

In our experiment, the amplitude of acceleration is set to be 1 g, and the sensitivity of the charge amplifier is set to 100 mV pC^{-1}. Each fiber is tested at 5, 10, 15, 20, 30, 40, 60, 80, 100, 150, 200, 250, 300, 350, 400, 450, and 500 Hz.

RESULTS AND DISCUSSION

An SEM view of a PVDF-coated fiber is shown in Figure 5. It can be clearly seen that by applying electric fields during fabrication, the diameter of the fiber varies little and the surface of the piezoelectric

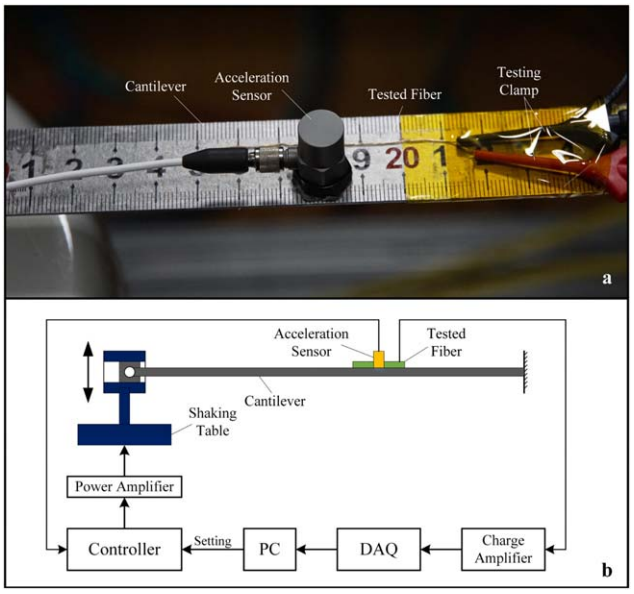

Figure 4. (a) Photo and (b) schematic of test setup. [Color figure can be viewed in the online issue, which is available at wileyonlinelibrary.com.]

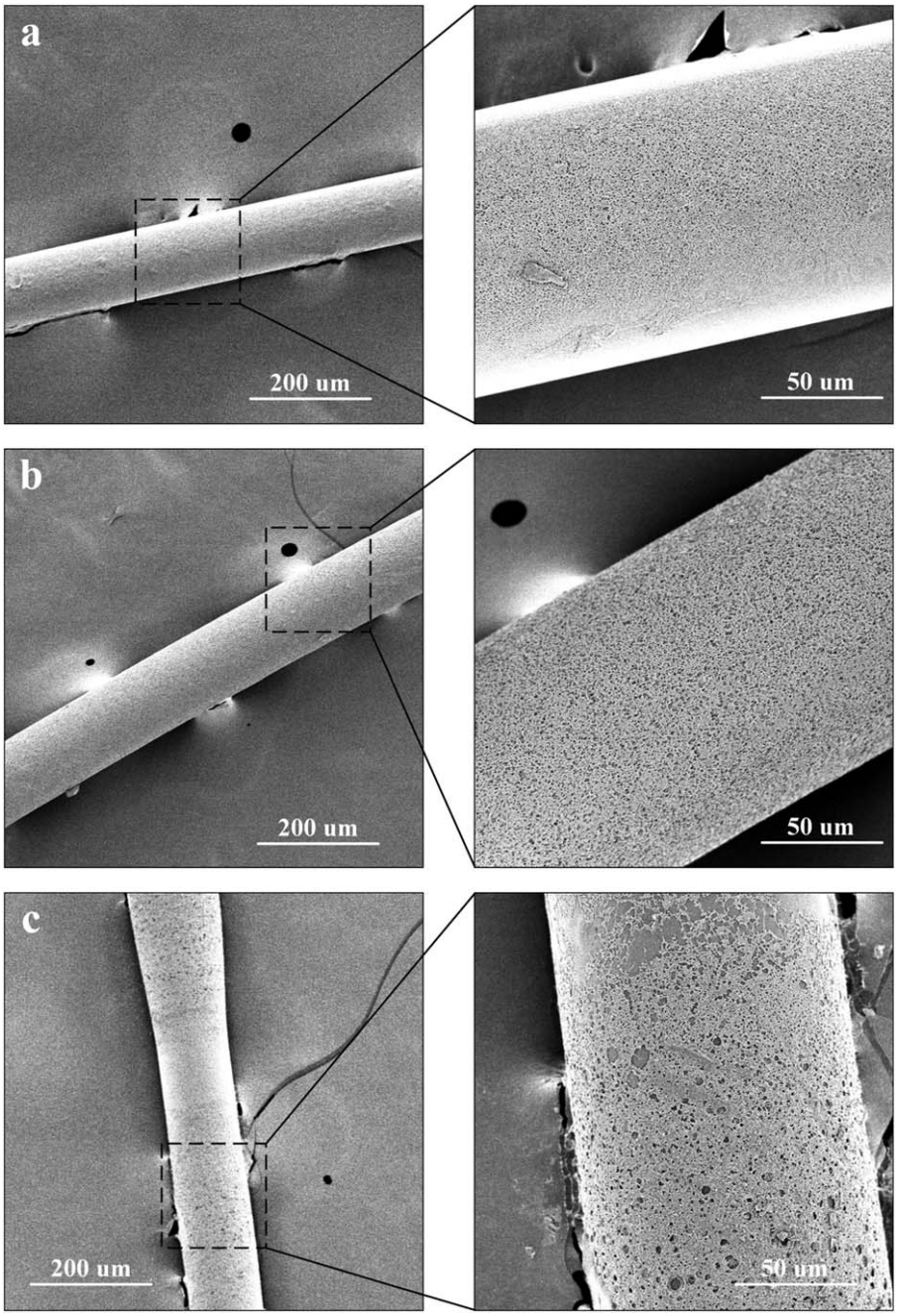

Figure 5. SEM view of (a) 15% PVDF coated fiber fabricated while applying electric fields, (b) 10% PVDF coated fiber fabricated while applying electric fields, and (c) 15% PVDF coated fiber fabricated without applying electric fields.

layer is continuous. Also it is noted that lots of porous structures are well distributed over the piezoelectric layer, and the diameters of the pores seem to decrease with the increasing PVDF concentration. This porous structure is considered to be generated in the evaporation of the solvent, and it enlarges the surface area of the fiber, which helps to increase the sensitivity in certain applications, for example, in gas sensors.

For the PVDF-TrFE coated fiber (shown in Figure 6), it is also seen that electric fields applied in fabrication help to improve the morphology of the piezoelectric layer. However, no obvious porous structure can be observed, which means the evaporation of the solvent affects the solidification of PVDF-TrFE less than for PVDF. This kind of fiber may be more suitable for applications that need a smooth surface, such as tactile sensors.

XRD patterns are shown in Figure 7. The 17.78°, 18.31°, and 20.03° peaks are alpha peaks of PVDF.[31] The 20.60° peak is the beta peak of PVDF.[31] The 20.35° peak is the beta peak of 70PVDF-30TrFE.[32] It is clearly shown that through electrowetting-aided dry spinning, the beta phase is formed in the PVDF layer, while the PVDF layer without any electric fields applied still shows the alpha phase. On the other hand, without solution charging caused by the first applied electric fields (V_1) on the copper needle, a significant but incomplete

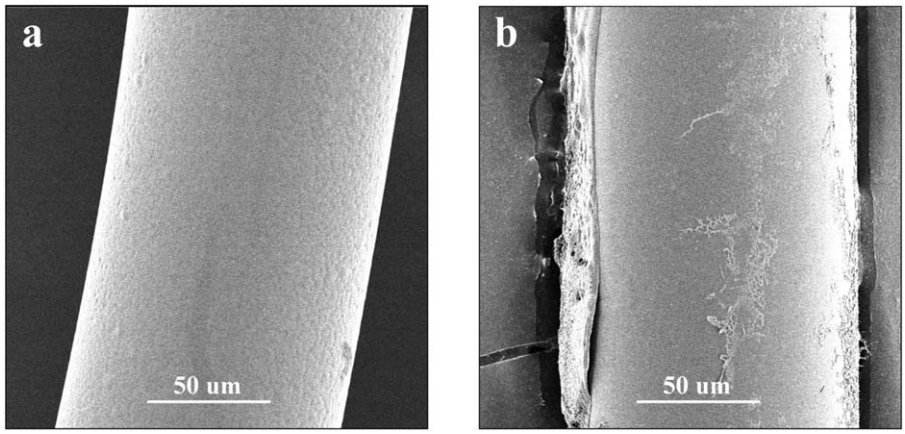

Figure 6. SEM view of 15% PVDF-TrFE coated fiber fabricated (a) while applying electric fields and (b) without applying electric fields.

beta phase transition can be observed in the PVDF layer. Which means, during the solidification of the solution, although the electric field is not as strong as the electric field needed for the complete beta phase transition of a solid PVDF structure, the second applied electric field (V_2) is still able to generate the beta phase in the PVDF layer under solidification. However, it should be noted that, compared to the fiber with solution charging, this transition is not complete, possibly due to the insufficient strength of the electric field. In other words, by driving the charged solution with an electric field, the elongation and further deforming processes also play important roles in forming the beta phase introduced by the electrowetting-aided dry spinning.

The thickness of the piezoelectric layers and other morphological properties are shown in Table I. It is observed that the thickness of each piezoelectric layer fabricated while applying electric fields retains much better consistency and varies less compared to that fabricated without applying electric fields. We can also see that with increasing concentration the thickness of the PVDF layer increases less than the PVDF-TrFE layer, while the dimension of the porous structure is decreasing.

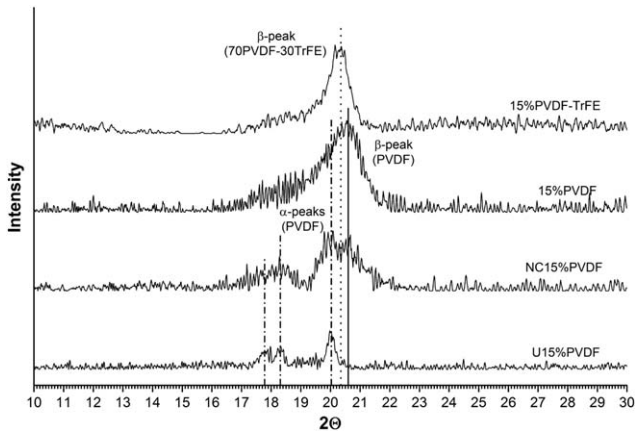

Figure 7. XRD patterns of 15% PVDF coated fiber fabricated without any electric fields applied (U15%PVDF), 15% PVDF coated fiber fabricated with electric fields applied only on copper electrodes (NC15%PVDF), 15% PVDF coated fiber fabricated with electric fields applied on copper needle and copper electrodes (15%PVDF), and 15% PVDF-TrFE coated fiber fabricated with electric fields applied on copper needle and copper electrodes (15%PVDF-TrFE).

The testing results for piezoelectric properties are shown in Figure 8. By comparison of the output voltage of the sensing fibers, it can be observed that the fibers fabricated without applying an electric field show much weaker response, mainly due to the unstable morphology of the piezoelectric layers, as well as the lack of a polarized piezoelectric dipole layer, due to missing the step of electric field–aided beta-phase formation and polarization. On the other hand, with increasing concentration, the outputs increase owing to shrinking of the porous structure in the PVDF layer and the increasing piezoelectric layer thickness. Finally, it can be also seen that the outputs of PVDF-TrFE coated fibers show relatively stronger response at low frequency compared to the PVDF ones.

In our experiment, as it is usually required to detect the vibration amplitude and frequency in practical applications, we define sensitivity as the value of the charge quantity at unit vibration amplitude. Thus we can draw the figures of sensitivity as in Figure 8(c) and Figure 8(d). A larger output at low frequency, which is shown in Figure 8(a) and Figure 8(b), is due

Table I. Morphological Properties of Piezoelectric Fiber

Fiber	Piezoelectric layer thickness (μm)	Main phase	Appearance
10%PVDF	6–9	Beta	Porous[a] (large)
15%PVDF	7–9	Beta	Porous (medium)
20%PVDF	8–9.5	Beta	Porous (small)
U15%PVDF[b]	3–32	Alpha	Fractured
10%PVDF-TrFE	3–5.5	Beta	Smooth[c]
15%PVDF-TrFE	5–7	Beta	Smooth
20%PVDF-TrFE	6.5–8	Beta	Smooth
U15%PVDF-TrFE[d]	2–28	Beta	Fractured

[a] Surface is continuous with porous structures (of different pore sizes) distributed on the fiber.
[b] 15% PVDF coated fiber fabricated without applying electric fields.
[c] Surface is continuous without porous structures distributed on the fiber.
[d] 15% PVDF-TrFE coated fiber fabricated without applying electric fields.

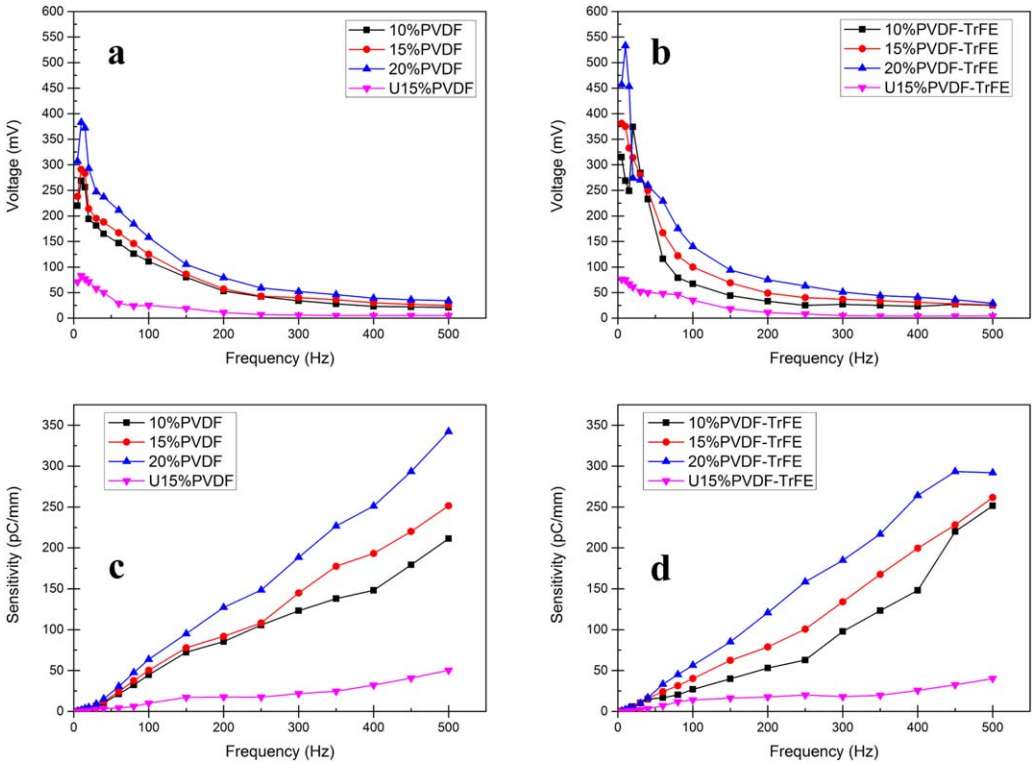

Figure 8. The voltage output of (a) PVDF coated fiber and (b) PVDF-TrFE coated fiber at acceleration of 1 g. The sensitivity of (c) PVDF coated fiber and (d) PVDF-TrFE coated fiber. U15%PVDF stands for 15% PVDF coated fiber fabricated without applying electric fields, and U15%PVDF-TrFE stands for 15% PVDF-TrFE coated fiber fabricated without applying electric fields. Sensitivity is defined as the value of charge at unit vibration amplitude. [Color figure can be viewed in the online issue, which is available at wileyonlinelibrary.com.]

to a larger vibration amplitude exerted because of the shaking characterization described in Eq. 1. From Figure 8(c) and Figure 8(d), it can be clearly seen that the sensitivity of the piezoelectric fiber increases with the frequency almost linearly, as described in Eq. 4, which also indicates that the generated charge quantity is almost linearly proportional to the strain of the fiber, and the fiber can perform better in higher frequency to detect vibration amplitude.

All the morphological and piezoelectric properties demonstrate that electrowetting-aided dry spinning helps to fabricate high-quality polymeric piezoelectric fibers. These fibers consist of a 100 μm copper core (enameled with 6 μm polyester-imide), a 3–10 μm piezoelectric layer, and sputtered 100 nm gold electrodes. Rather than directly extruding the polymeric melt onto a solid surface, this piezoelectric layer is more closely attached with the help of electrowetting during the fabrication. Because the polymeric layer is much thinner than the copper core, most of the stress concentrates on the metal core, which means the mechanical behavior of this fiber performs linearly, almost the same as a metal wire. That simplifies signal processing in sensing applications.

CONCLUSIONS

Morphologically stable piezoelectric fibers with a metal core and a beta-phase PVDF (or PVDF-TrFE) layer are fabricated by an electrowetting-aided dry spinning method. The beta phase transition as well as polarization of the piezoelectric layer is achieved through electric fields applied in the piezoelectric layer under solidification. The morphological properties of the fibers are analyzed through SEM, XRD, and a step profiler, while the piezoelectric properties are tested in a vibration-detecting application, which all demonstrate the stable performance of these fibers. The electrowetting-aided dry spinning method can also be applied in other fabrications to enhance adhesion between the liquid and the solid surface.

ACKNOWLEDGMENTS

This work was supported in part by the National Basic Research Program (973) of China (2011CB013303), the National Natural Science Foundation of China (51521064), and the Applied Research Project of Public Welfare Technology of Zhejiang Province (2015C31109).

REFERENCES

1. Qiu, J.; Tani, J.; Yamada, N.; Takahashi, H. *Proc. SPIE* **2003**, *5053*, 475.
2. Sato, H.; Sekiya, T.; Nagamine, M. *Proc. SPIE* **2004**, *5390*, 97.
3. Sebald, G.; Qiu, J.; Guyomar, D. *J. Phys. D. Appl. Phys.* **2005**, *38*, 3733.
4. Sato, H.; Nagamine, M. *Proc. SPIE* **2005**, *5764*, 623.

5. Takagi, K.; Sato, H.; Saigo, M. *Proc. SPIE* **2005**, *5757*, 471.
6. Takagi, K.; Sato, H.; Saigo, M. *Proc. SPIE* **2004**, *5383*, 376.
7. Yanaseko, T.; Asanuma, H.; Chiba, T.; Takeda, N.; Sato, H. *Trans. Mater. Res. Soc. Japan* **2014**, *39*, 325.
8. Yanaseko, T.; Asanuma, H.; Sato, H. *Mech. Eng. J.* **2015**, *2*, 14-00357.
9. Tajitsu, Y.; Chiba, A.; Furukawa, T.; Date, M.; Fukada, E. *Appl. Phys. Lett.* **1980**, *36*, 286.
10. Zhang, Q. M.; Bharti, V.; Zhao, X. *Science* **1998**, *280*, 2101.
11. Chu, B.; Zhou, X.; Ren, K.; Neese, B.; Lin, M.; Wang, Q.; Bauer, F.; Zhang, Q. M. *Science* **2006**, *313*, 334.
12. Rathod, V. T.; Mahapatra, D. R.; Jain, A.; Gayathri, A. *Sens. Actuators, A* **2010**, *163*, 164.
13. Nilsson, E.; Lund, A.; Jonasson, C.; Johansson, C.; Hagström, B. *Sens. Actuators, A* **2013**, *201*, 477.
14. Lund, A.; Hagström, B. *J. Appl. Polym. Sci.* **2010**, *120*, 1080.
15. Lund, A.; Jonasson, C.; Johansson, C.; Haagensen, D.; Hagström, B. *J. Appl. Polym. Sci.* **2012**, *126*, 490.
16. Glauß, B.; Steinmann, W.; Walter, S.; Beckers, M.; Seide, G.; Gries, T.; Roth, G. *Materials (Basel)* **2013**, *6*, 2642.
17. Bian, Y.; Liu, R.; Hui, S. *Funct. Mater. Lett.* **2015**, *9*, 1650001.
18. Kechiche, M. B.; Bauer, F.; Harzallah, O.; Drean, J. Y. *Sens. Actuators, A* **2013**, *204*, 122.
19. Grujicic, M.; Sellappan, V.; Omar, M. A.; Seyr, N.; Obieglo, A.; Erdmann, M.; Holzleitner, J. *J. Mater. Process. Technol.* **2008**, *197*, 363.
20. Dolay, A.; Courtois, C.; D'Astorg, S.; Rguiti, M.; Petitniot, J.-L.; Leriche, A. *J. Eur. Ceram. Soc.* **2014**, *34*, 2951.
21. Vallet, M.; Berge, B.; Vovelle, L. *Polymer (Guildf)* **1996**, *37*, 2465.
22. Vallet, M.; Vallade, M.; Berge, B. *Eur. Phys. J. B* **1999**, *11*, 583.
23. Quilliet, C.; Berge, B. *Curr. Opin. Colloid Interface Sci.* **2001**, *6*, 34.
24. Hong, J. S.; Ko, S. H.; Kang, K. H.; Kang, I. S. *Microfluid. Nanofluid.* **2008**, *5*, 263.
25. Ricks-Laskoski, H. L.; Buckley, M. A.; Snow, A. W. *J. Appl. Polym. Sci.* **2008**, *110*, 3865.
26. Andrew, J. S.; Clarke, D. R. *Langmuir* **2008**, *24*, 670.
27. Salimi, A.; Yousefi, A. A. *Polym. Test.* **2003**, *22*, 699.
28. Samara, G. A.; Bauer, F. *Ferroelectrics* **1992**, *135*, 385.
29. Das-Gupta, D. K.; Doughty, K. *J. Appl. Phys.* **1978**, *49*, 4601.
30. Giacometti, J. A.; Ribeiro, P. A.; Raposo, M.; Marat-Mendes, J. N.; Carvalho Campos, J. S.; DeReggi, A. S. *J. Appl. Phys.* **1995**, *78*, 5597.
31. Wang, Y.; Cakmak, M.; White, J. L. *J. Appl. Polym. Sci.* **1985**, *30*, 2615.
32. Latour, M. *Key Eng. Mater.* **1994**, *92*, 31.